

A receiver-side power control method for series-series magnetic topology in inductive contactless electric vehicles battery charger application

Bhukya Bhavsingh¹, Gotluru Suresh Babu², Bhukya Mangu³, Ravikumar Bhukya¹

¹Department of Electrical Engineering, Faculty of Electrical Engineering, Rajiv Gandhi University of Knowledge Technologies Basar, Telangana, India

²Department of Electrical and Electronics Engineering, Faculty of Electrical Engineering, Chaitanya Bharathi Institute of Technologies, Telangana, India

³Department of Electrical Engineering, Faculty of Engineering, University College of Engineering, Osmania University, Telangana, India

Article Info

Article history:

Received Feb 15, 2023

Revised Mar 24, 2023

Accepted Jun 26, 2023

Keywords:

Bidirectional switches

Electrical vehicle

Power regulation methods

S/S compensation

ABSTRACT

Wireless power transfer (WPT) can be used to charge the battery conveniently and efficiently. In this paper, the investigation of high-efficiency S/S resonant magnetic topology in inductive wireless battery charging of electric vehicles (EVs) is analyzed, designed, and controlled. To regulate the output power efficiently rather than controlling the supply voltage, novel bidirectional switches are introduced to control the output power by using the duty cycle control method. The output power of the secondary side is derived and discussed based on the fundamental harmonic approximation (FHA) approach. A 1.5 kW, 120 mm distance, and 85 kHz resonance frequency are verified in MATLAB/Simulink.

This is an open access article under the [CC BY-SA](https://creativecommons.org/licenses/by-sa/4.0/) license.



Corresponding Author:

Bhukya Bhavsingh

Department of Electrical Engineering, Faculty of Electrical Engineering,

Rajiv Gandhi University of Knowledge Technologies Basar

Nirmal District, Telangana, 504107, India.

Email: bhavsingh.eee@rgukt.ac.in

1. INTRODUCTION

In the current generation, greenhouse gas emissions and fossil pollution have become big issues [1]–[3]; these can be overcome by using renewable energy sources as the best solution, plug-in hybrid electric vehicles (PHEVs) and electric vehicles (EVs). So the usage of PHEVs and battery-operated electric vehicles EVs has dramatically increased [4]–[7]. The traditional plug-in charging path is not convenient and sometimes unsafe; also this is the main reason for promoting and applying plug-in hybrid EVs and EVs. Wireless power transfer (WPT) system has many advantages like high reliability, flexibility, and security [8], [9]. It is accepted as a preferred technology for the charging of EVs in tailless TV; wireless flat-panel chargers designed for suitable electronic products, biomedical devices, and academia. The research in WPT systems is concentrated on coil design, compensation circuits, battery management systems, power transfer efficiency (PTE), and control techniques.

Figure 1 depicts the typical wireless EV charging system, this tells about several stages for charging an EV without any contact. The transmitter side will be on the ground and the receiver's side will be in the vehicle. To get supply to the transmitter side, the utility grid of alternating current (AC) supply is converted

to direct current (DC), such that constant DC voltage is given to the high-frequency DC to the AC basic H-bridge inverter [10], [11]. The sending and receiver coil in the WPT system has weak coupling because of the distance between vehicle ground clearances. For this reason, the reactive power input requirement increases. This has a direct effect on decreasing power transfer capability as well as increasing of rating of the converter circuit. But in the literature, as time passes several compensation topologies have developed to achieve near zero input reactive power. A capacitor is added on both sides of the WPT system in different combinations such as series-series (S-S), series-parallel (S-P), parallel-parallel (P-P), and parallel-series (P-S) in that S-S, S-P [12]–[14] are voltage-fed compensators. P-P and P-S are current-fed compensators. Therefore to achieve the zero input reactive power, the input impedance will be almost resistive which results in zero phase angle (ZPA) [15] between input current and voltage. So power transfer capability (PTC) and efficiency of the WPT system will increase. Figure 1 represents the basic structure of the EV charger that has parts: i) the contactless primary and secondary coils, ii) the resonance network, iii) the power electronics components, and iv) filter circuits.

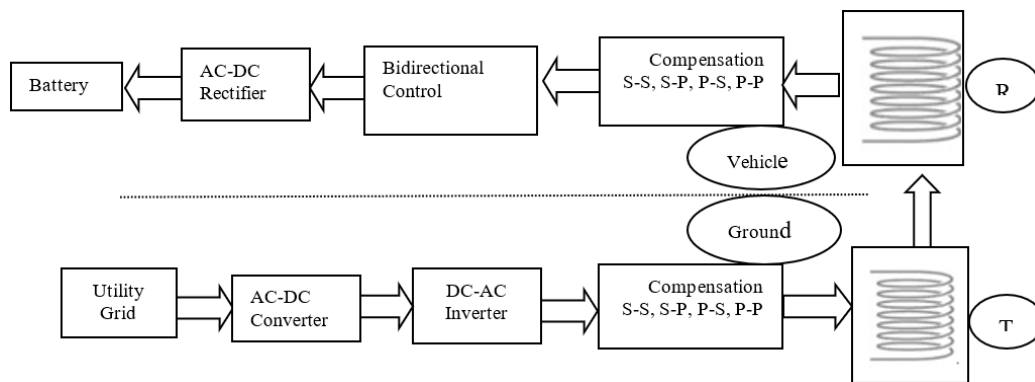


Figure 1. WPT system with S-S compensation

In a wireless system, the basic parameter is the distance between the ground and the vehicle and the alignment of the coils. So, the typical coupling coefficient is 20% to 30%, it is directly affected by the transferred power and efficiency. So it requires compensation on both sides of the coils. Among these four basic compensation circuits, only the S/S compensation circuit, which was analyzed in detail in [16]–[20], is reliable, flexible, and has fewer components compared to other topology costs.

To transfer the maximum power and increase the performance, the four compensation circuits and control methods like phase shift control strategy (PSC) [21], [22], pulse width modulation (PWM) strategy [23], frequency control (FC) strategy [24], [25], and DC/DC converters have been discussed [26]. However, in the S-S compensation method, the DC/DC converter is placed on the primary side. In that connection the load side parameters vary, so to avoid this complexity the closed loop method is required, but again cost and smooth operation constraints, proposed novel bidirectional switches connected in the secondary side before the rectifier. It can be operated by using the duty cycle control methods in the S-S compensated wireless power transfer system and is discussed purely on the fundamental harmonic approximation (FHA) method.

The rest of the paper is categorized as follows. The model and basic S/S resonance circuit are analyzed in section 2, the proposed S/S resonance circuit operation and design are presented in section 3, the simulated results of an S/S resonance WPT are presented in section 4, experimental verification in section 5, and last, the conclusions section 6.

2. FUNDAMENTAL HARMONIC APPROXIMATION ANALYSIS OF EXISTING S/S COMPENSATION CIRCUIT

Figure 2 shows the S/S compensation electrical circuit, Figure 2(a) represents the primary and secondary coils network with their respective compensation, and Figure 2(b), using Kirchoff's voltage law (KVL) and by considering the coil resistance R_1 and R_2 , I_1 and I_2 can be written as (1) and (2).

$$V_{AB} = \left(R_1 + j\omega L_1 + \frac{1}{j\omega C_1} \right) I_1 - j\omega M I_2 \quad (1)$$

$$j\omega M I_1 = \left(R_2 + j\omega L_2 + \frac{1}{j\omega C_2} \right) I_2 + R_{ac} I_2 \tag{2}$$

Where $Z_1 = R_1 + j\omega L_1 + \frac{1}{j\omega C_1}$ and $Z_2 = R_2 + j\omega L_2 + \frac{1}{j\omega C_2}$

From (1) and (2) we can get (3) and (4).

$$V_{AB} = Z_1 I_1 - j\omega M I_2 \tag{3}$$

$$j\omega M I_2 = Z_2 I_2 + I_2 R_{ac} = (Z_2 + R_{ac}) I_2 \tag{4}$$

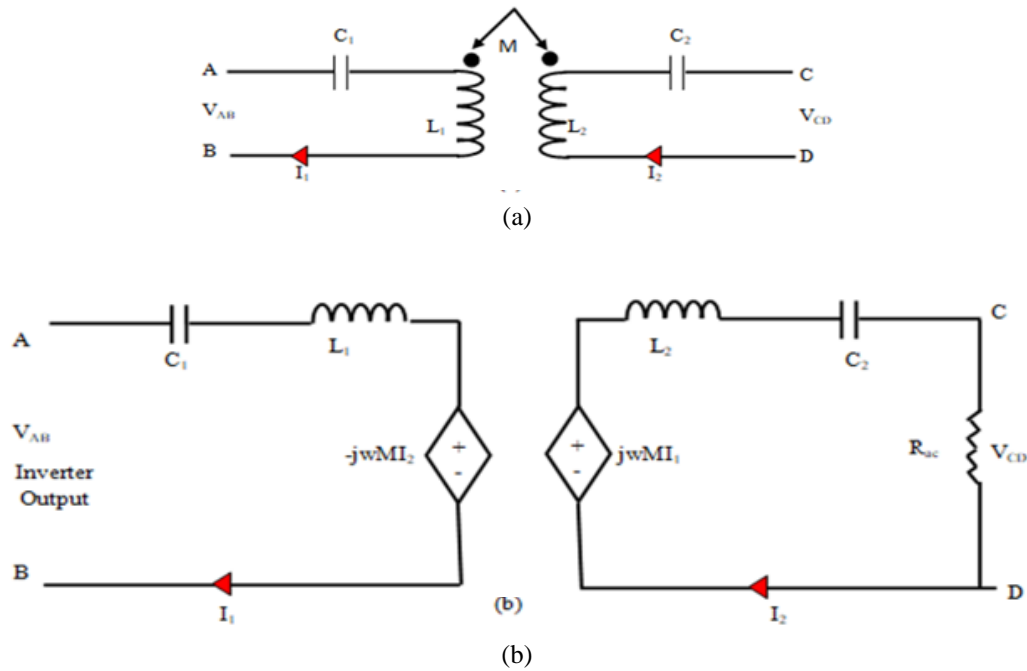


Figure 2. S/S compensation electrical circuit (a) equivalent circuit (b) voltage-dependent circuit

From (4), the receiver's current I_2 can be written as (5).

$$I_2 = \frac{j\omega M I_1}{Z_2 + R_{ac}} \tag{5}$$

Sub (5) in (3), we get transmitter current I_1

$$\begin{aligned} V_{AB} &= Z_1 I_1 - j\omega M I_1 \left(\frac{j\omega M I_1}{Z_2 + R_{ac}} \right) \\ V_{AB} &= \left(Z_1 + \frac{\omega^2 M^2}{Z_2 + R_{ac}} \right) I_1 \Rightarrow \left(\frac{Z_1 Z_2 + Z_1 R_{ac} + \omega^2 M^2}{Z_2 + R_{ac}} \right) I_1 \\ I_1 &= \frac{V_{AB} (Z_2 + R_{ac})}{Z_1 (Z_2 + R_{ac}) + (\omega M)^2} \end{aligned} \tag{6}$$

Sub (6) in (5), we get the current I_2

$$\begin{aligned} I_2 &= \frac{j\omega M}{(Z_2 + R_{ac})} \left(\frac{V_{AB} (Z_2 + R_{ac})}{Z_1 (Z_2 + R_{ac}) + (\omega M)^2} \right) \\ I_2 &= \frac{j\omega M V_{AB}}{Z_1 (Z_2 + R_{ac}) + (\omega M)^2} \end{aligned} \tag{7}$$

In the above equation, Z_1 and Z_2 are the impedance of the transmitter and receiver side, V_{AB} is the inverter output voltage, equivalent load resistance $R_{ac} = \frac{8}{\pi^2} R_L$. The M is calculated through the coupling factor k and the self-inductances L_1 and L_2 as in (8) and compensating capacitors C_1 and C_2 as in (9). In Figure 3 the receiver output voltage between points C and D is supplied to the full bridge rectifier, the rectified supply is filtered by using a suitable filter circuit connected to the battery, and the battery gets charged. By KVL and the V_{AB} taken as the reference and at resonance, $X_L = X_C$, the neglected coil resistance in Figure 3 can be drawn as Figure 4.

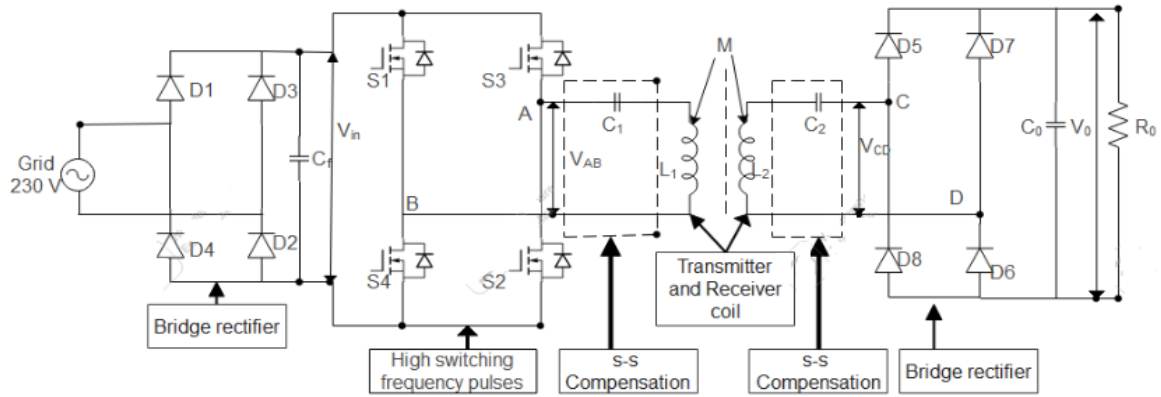


Figure 3. Structure of the WPT system

$$M = k\sqrt{L_1 L_2} \tag{8}$$

$$\begin{cases} C_1 = \frac{1}{\omega_0^2 L_1} \\ C_2 = \frac{1}{\omega_0^2 L_2} \end{cases} \tag{9}$$

$$R_L = V_0 / I_0 \tag{10}$$

Where V_0 is the output voltage, I_0 is the output current, R_L is the equivalent load resistance.

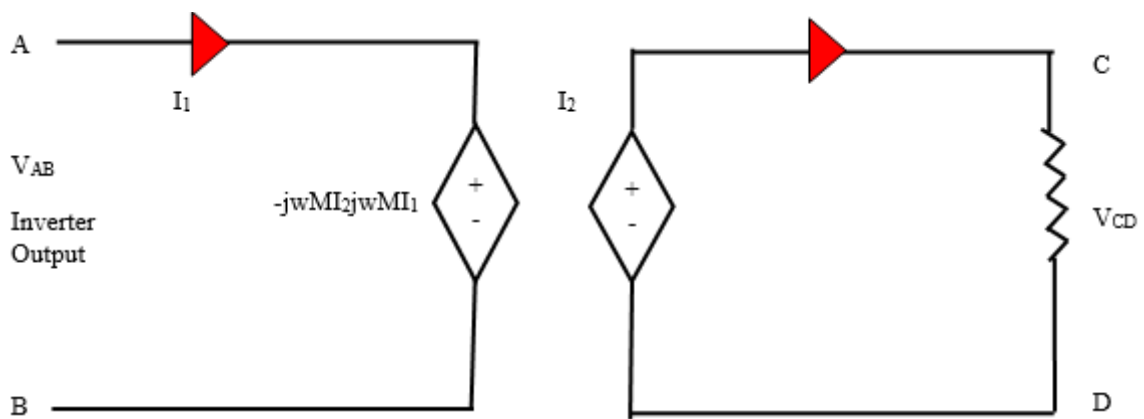


Figure 4. Resonance voltage-dependent equivalent circuit

Apply ohms law on the transmitter and receiver side, $V_{AB} = j\omega_0 M I_2$

$$I_2 = \frac{V_{AB}}{-j\omega_0 M} = \frac{V_{AB}}{\omega_0 M} \angle 90^\circ \tag{11}$$

$$j\omega_0 M I_1 = R_{ac} I_2 = V_{CD} \tag{12}$$

Sub (8) in (9), we get I_1

$$I_1 = \frac{R_{ac}}{j\omega_0 M} I_2 \tag{13}$$

$$I_1 = \frac{V_{CD}}{j\omega_0 M} = \frac{V_{CD}}{j\omega_0 M} \angle 0^\circ \tag{14}$$

$$I_1 = \frac{V_{AB} R_{ac}}{(w_0 M)^0} = \frac{V_{AB} R_{ac}}{(w_0 M)^2} < 0^\circ$$

Receiver current I_2 can be found in (11), that the RMS value is independent of the output voltage (V_{CD}), also it depends on the supply voltage (V_{AB}), and mutual inductance (M). The S/S compensated wireless charger is a constant current source and can be controlled by the supply voltage in general [27]–[31]. The P_{out} and P_{in} real power can be obtained as (15) [32].

$$P_{out} = P_{in} = \text{Re}(V_{AB} I_1^*) = \frac{1}{w_0 M} V_{AB} V_{CD} \tag{15}$$

Measurements of coils' mutual inductance concerning distance are shown in Table 1. When the distance between the transmitter and receiver coils varies, accordingly coupling coefficient and mutual inductance vary [33]. Figure 5 shows the coupling coefficient (k) decreases fast when the distance rises and the mutual inductance decreases as well as the PTC also decreases.

Table 1. Distance and coupling coefficient concerning mutual inductance

Distance (mm)	Coupling coefficient (k)	Mutual Inductance (μH)
50	0.6	235.54
100	0.24	94.21
120	0.16	62.9
150	0.10	39.2
200	0.05	19.6

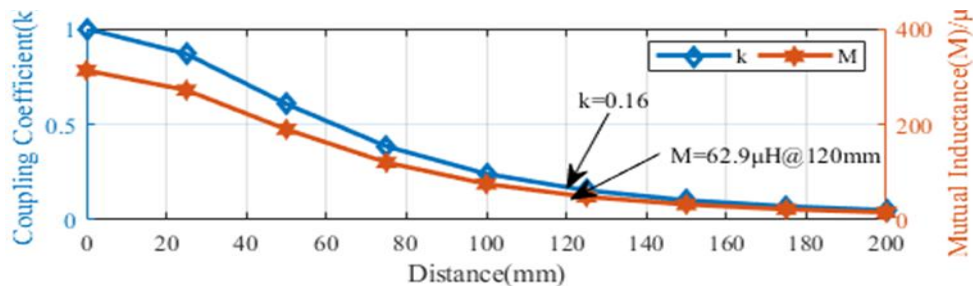


Figure 5. Coupling coefficient and mutual inductance with the distance between the primary coil and secondary coil

Figures 6 (a, b, c, d, and e) show the transfer power as a function of the supply voltage for five coupling factors and four output voltages. Various coupling factors are studied by adjusting the air gap and misalignment between primary and secondary side coils. The output power varies linearly with the supply voltage. The same thing will happen in low supply voltage and low coupling situations.

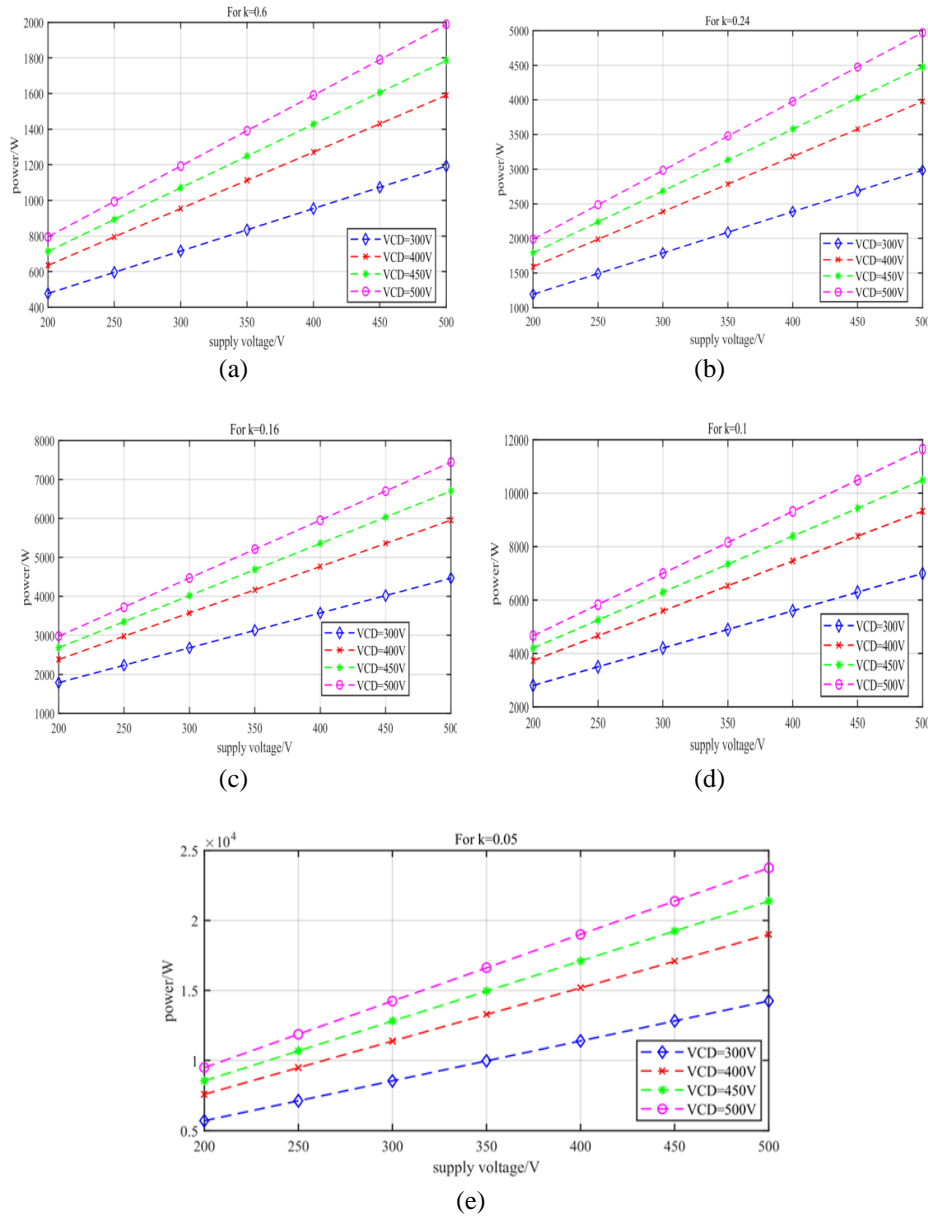


Figure 6. Transferred power for the designed system at (a) k = 0.6, (b) k =0.24, (c) k =0.16, (d) k =0.1, and (e) k =0.05

3. PROPOSED TOPOLOGY AND ANALYSIS

According to the waveform of the inverter output voltage (V_{AB}) and rectifier input voltage (V_{CD}). It can be obtained by the Fourier series as (16) and (17) [34]–[36].

$$V_{AB} = \sum_{k=1}^{\infty} \frac{4}{(2k+1)\pi} V_{AB} \sin((2k + 1)\omega_0 t) \tag{16}$$

$$V_{CD} = \sum_{k=1}^{\infty} -\frac{4}{(2k+1)\pi} V_{CD} \sin\left(\frac{2k+1}{2}(\pi - \alpha)\right) \cos((2k + 1)\omega_0 t) \tag{17}$$

By substituting (16) and (17) into (15), the output power P_{out} can also be derived, where the duty cycle $D = \alpha/\pi$.

$$P_{out} = \frac{V_{AB} * V_{CD} * 8}{\pi^2 \omega_0 M} \sum_{k=0}^{\infty} \frac{\sin\left(\left(\frac{2k+1}{2}\right)\pi(1-D)\right)}{(2k+1)^3} \tag{18}$$

The basic structure of the S-S compensation model can be modified by adding two bidirectional switches S_5 and S_6 inserted before an uncontrolled rectifier to control the output power by varying the duty cycle of the switches as shown in Figure 7.

Operating modes, the input and output voltage waveforms along with the pulses given to the bidirectional switches S_5 and S_6 with pulse width α are shown in Figure 8. One operation period consisting of successive modes. The direction of current in a half cycle, having four modes of the fundamental frequency of input or output voltage directions is shown in Figure 9.

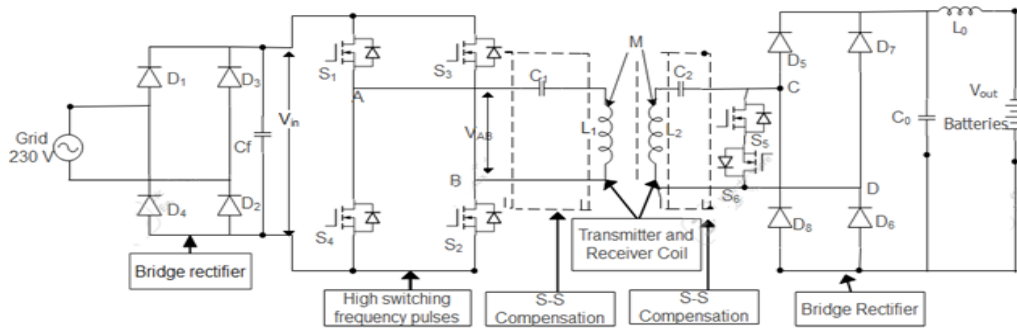


Figure 7. Secondary side power control WPT system

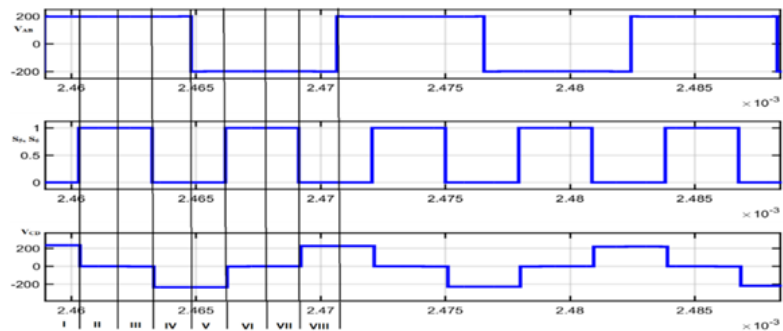


Figure 8. Bidirectional switches operating waveform

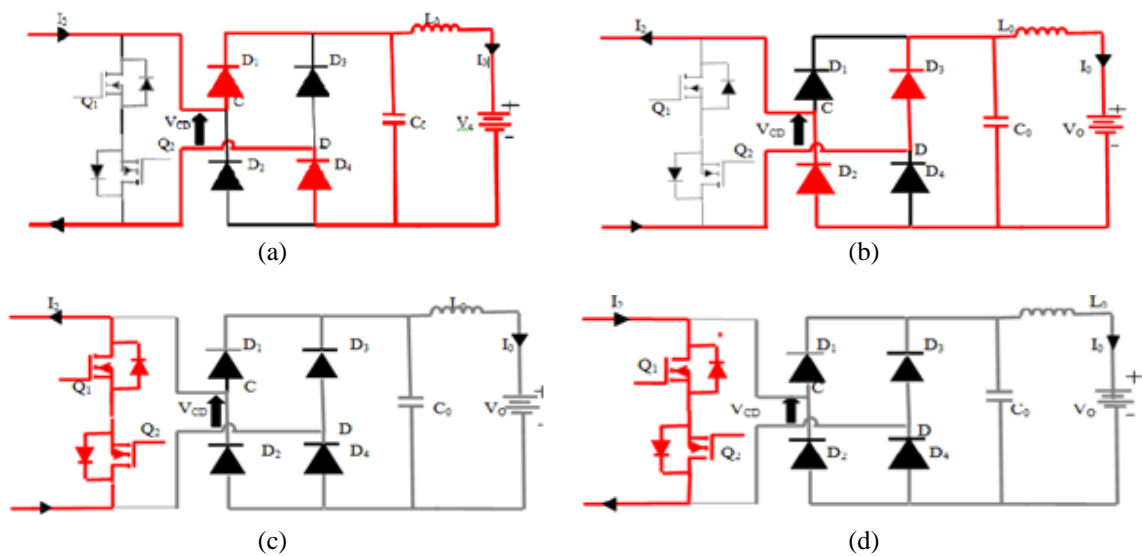


Figure 9. Current flow direction in the secondary-side control method (a) Mode I (b) Mode II (c) Mode III (d) Mode IV

According to Figure 9, Mode-I operates from $\omega t = 0$ to $\omega t = (\pi/2) - (\alpha/2)$. The two control switches S_5 and S_6 are turned off. The output current i_r enters through diode D_5 and leaves through D_6 . Since the battery voltage is fixed, the output voltage V_{CD} is equal to V_{out} . Mode-II is in between $\omega t = (\pi/2) - (\alpha/2)$ to $\omega t = \pi/2$. The two control switches S_5 and S_6 are turned on. The output current i_r flows through S_5 and S_6 . It makes the voltage V_{CD} zero. In this mode, the battery won't charge. Mode-III it operates from $\omega t = \pi/2$ to $\omega t = (\pi/2) + (\alpha/2)$. The two control switches S_5 and S_6 are still on, the output I_2 passes during switches S_5 and S_6 . The current direction is opposite to the current direction in mode II. Since the switches are short-circuited on the secondary side, the output voltage V_{CD} is zero, as well as the battery is not charged. Mode-IV it operates from $\omega t = (\pi/2) + (\alpha/2)$ to $\omega t = \pi$. The two control switches S_5 and S_6 are turned off. In this mode, the current i_r enters through diode D_7 and leaves through diode D_8 . The battery gets charged and the output voltage V_{CD} is equal to V_{out} .

From Figure 8, the modes V, VI, VII, and VIII belong to the second cycle of the gate pulses and are the same as the first half cycle, the same operation principle will be repeated for the next cycle of the operating waveforms.

4. RESULTS AND DISCUSSION

Simulated parameters, as per the wireless standards of SAEJ2954 standards allow, the frequency range is 85 kHz, the quality factor (Q) is 6, for bifurcation-free operation [37], [38] coupling coefficient $k = 0.16$ at an air gap of 120 mm, calculate the parameters are $L_1 = 325\mu\text{H}$, $L_2 = 474.22\mu\text{H}$, $M = 62.9\mu\text{H}$, $C_1 = 10.79\text{nF}$, $C_2 = 7.4\text{nF}$, $V_{AB} = 200\text{V}$, $V_{CD} = 280$. By using the proposed method, the evaluated parameter is inserted in MATLAB simulation, We observed that the duty cycle D increased from $d = 0$ to 1, as the output power P_{out} decreased. When duty cycle D goes to 1, terminals C and D are short-circuited, and the output power is zero. It reduces the controlling complexity and strengthens the control stability. When D is greater than 0.5, the output power reduced is fast with the rise of D, which means the P_{out} is controlled effectively and it is easier when D is in between 0 and 0.5.

Comparison of input voltage and current of the primary side and output voltage and current of the secondary side. From the above Figures 10(a) and (b) to 15(a) and (b) comparison, it can be concluded that, even after the changing of the duty cycle from $d = 0$ to $d = 1$, the receiver side voltage and power can be controlled but not the variation of transmitting parameters. Figure 16, shows the simulation results for duty cycle $D = 0$, Figure 16(a) shows output voltage and current, Figure 16(b) shows output power, and Figure 16(c) shows rectifier output current also studied.

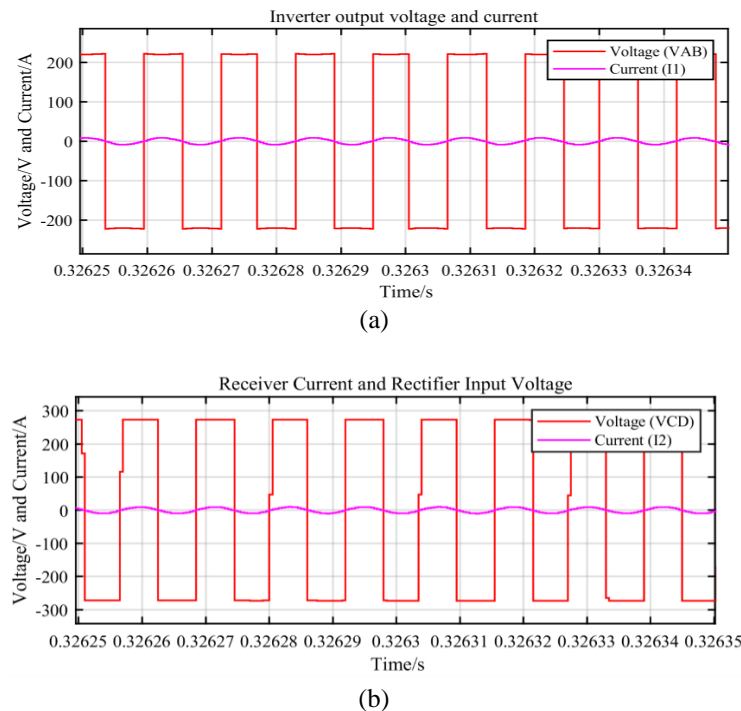
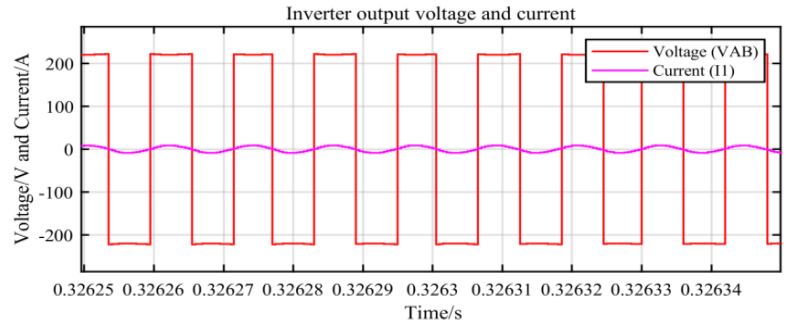
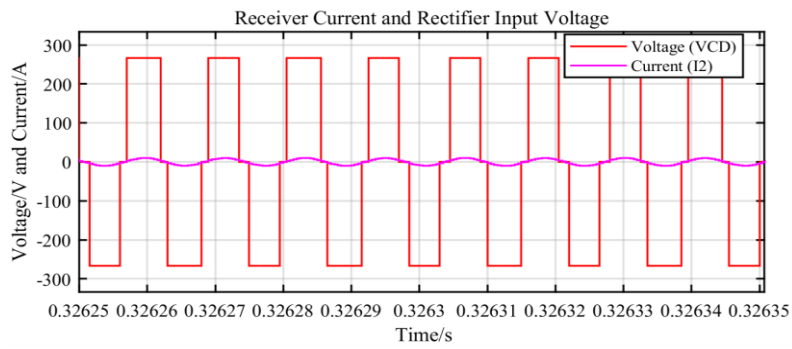


Figure 10. Comparison of input voltage and current of the primary side and output voltage and current of the secondary side, (a) Inverter VAB and I1 and (b) Rectifier VCD and I2 at a duty cycle $d = 0$

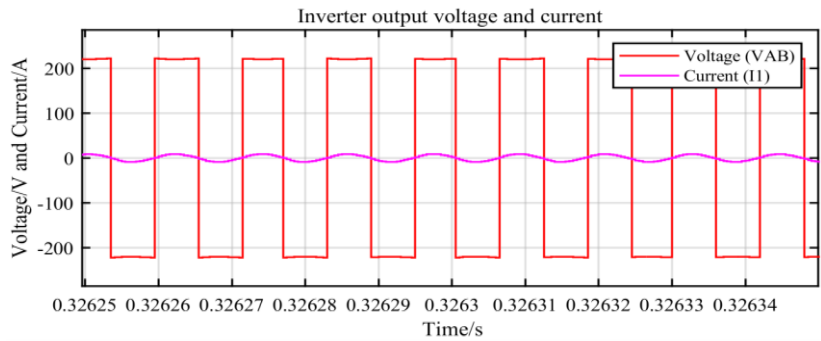


(a)

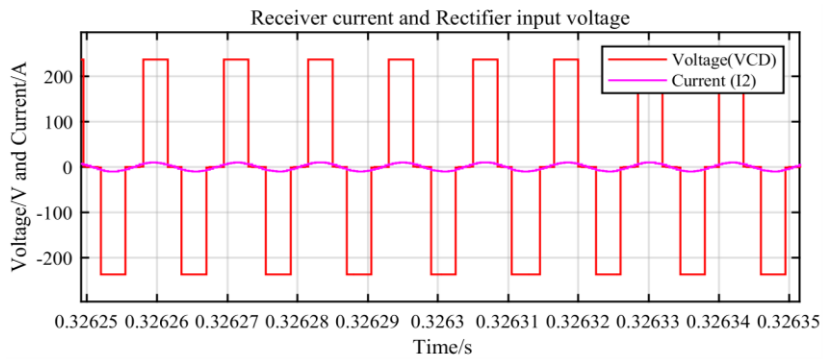


(b)

Figure 11. Comparison of input voltage and current of the primary side and output voltage and current of the secondary side, (a) Inverter V_{AB} and I₁ and (b) Rectifier V_{CD} and I₂ at a duty cycle d=0.2



(a)



(b)

Figure 12. Comparison of input voltage and current of the primary side and output voltage and current of the secondary side, (a) Inverter V_{AB} and I₁ and (b) Rectifier V_{CD} and I₂ at a duty cycle d=0.4

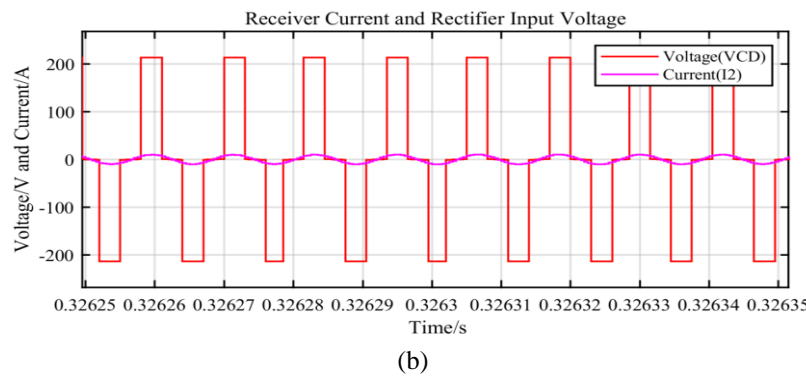
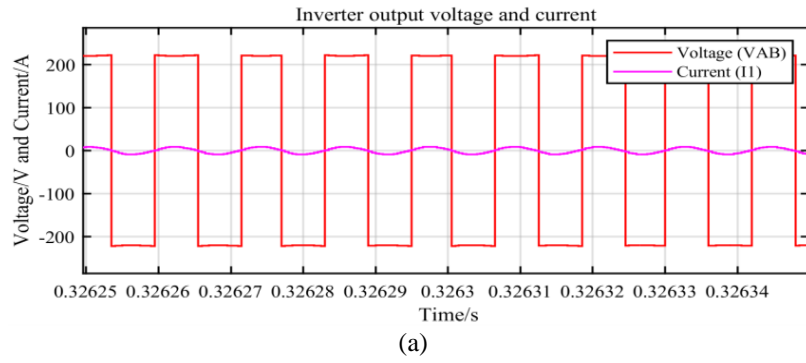


Figure 13. Comparison of input voltage and current of the primary side and output voltage and current of the secondary side, (a) Inverter V_{AB} and I_1 and (b) Rectifier V_{CD} and I_2 at a duty cycle $d=0.5$

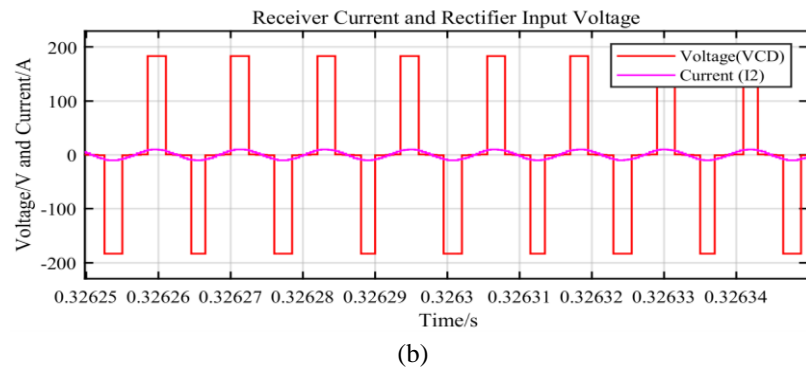
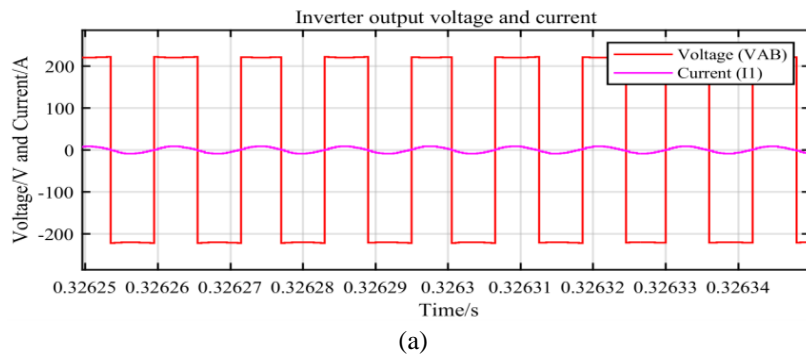
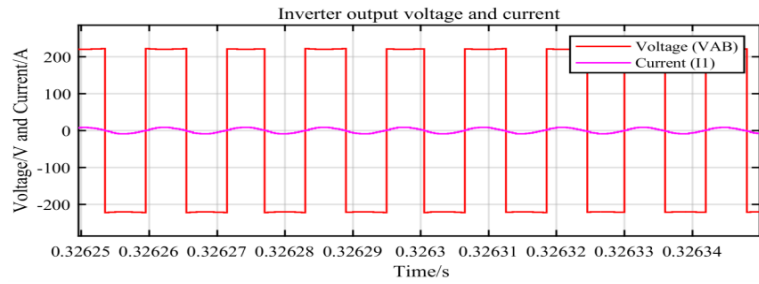
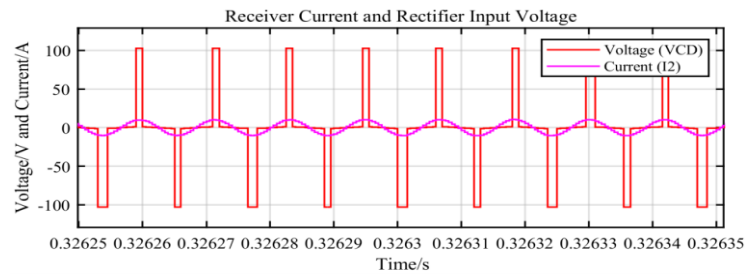


Figure 14. Comparison of input voltage and current of the primary side and output voltage and current of the secondary side, (a) Inverter V_{AB} and I_1 and (b) Rectifier V_{CD} and I_2 at a duty cycle $d=0.6$

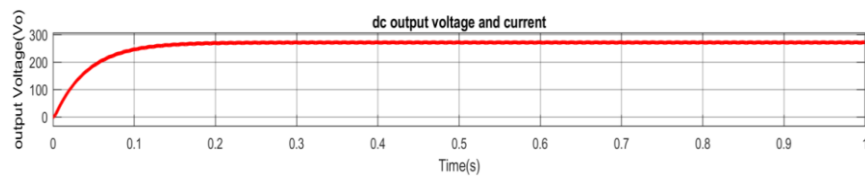


(a)

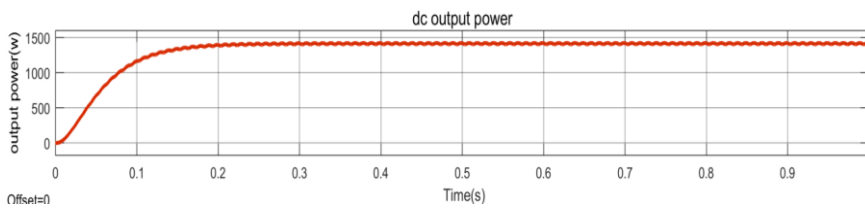
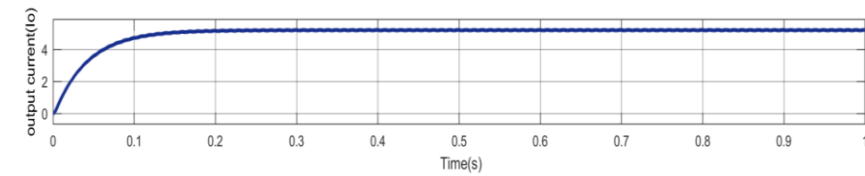


(b)

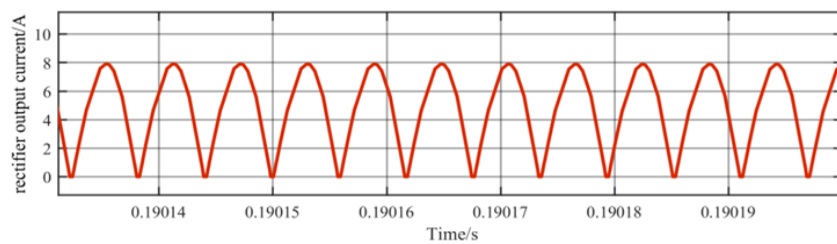
Figure 15. Comparison of input voltage and current of the primary side and output voltage and current of the secondary side, (a) Inverter V_{AB} and I_1 and (b) Rectifier V_{CD} and I_2 at a duty cycle $d=0.8$



(a)



(b)



(c)

Figure 16. The simulation results for duty cycle $D = 0$ of (a) DC output voltage and current, (b) DC output power, and (c) rectification bridge output current i_0 (A)

Figure 17 shows the simulation results for duty cycle $D = 0.5$, Figure 17(a) shows the inverter output voltage and transmitter current, Figure 17(b) shows the output voltage and current power, and Figure 17(c) shows the rectifier output current.

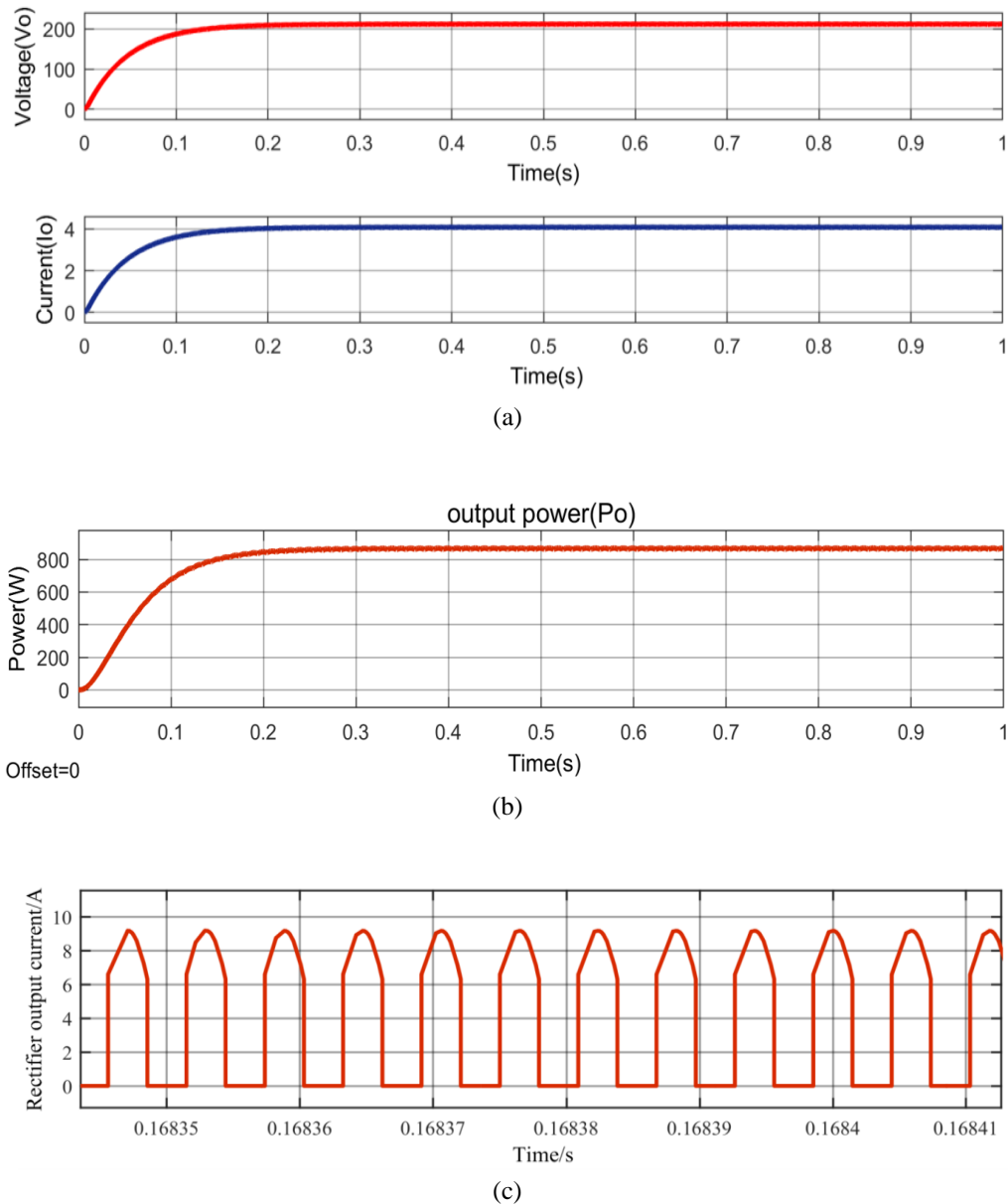


Figure 17. The simulation results for duty cycle $D = 0.5$ of (a) DC output voltage and current, (b) DC output power, and (c) Rectification bridge output current $i_0(A)$

Comment: i) When the duty cycle $D = 0$, in the S/S WPT system, the output current, voltage, power, and transmitter currents are the maximum values; ii) When the duty cycle $D = 0.5$, the output current, output voltage, output power, and transmitter current are approximately half; and iii) As the duty cycle increases from $D = 0$ to $D = 1$, the output power/W decreases. Figure 18 shows the transmitted power and duty cycle are also simulated. Table 2 shows the mathematical and simulated output power is the same concerning duty cycle variation.

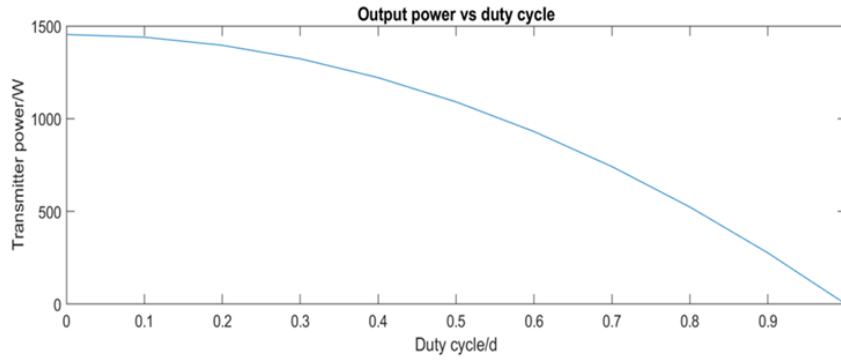


Figure 18. Output power versus duty cycle

Table 2. The system efficiency, power, and duty cycle D change with S_5 and S_6

Duty cycle D	Output Power/W		Efficiency	Conducting angle (α) = $D \cdot \pi$ (deg)
	Mathematical	Simulated		
0	1353.28	1421	96	0
0.4	1094.83	1075	95.44	72
0.5	956.91	869.3	95.26	90
0.6	795.44	638.7	95.02	108
0.8	418.188	228	92.28	144
1	0	0	-	180

5. EXPERIMENTAL VERIFICATION

A 1.5 kW prototype is designed, based on the basic topology as shown in Figure 3. The length of the transmitter and receiver coils is 400 mm × 400 mm, and the ground clearance is 120 mm. The transmitter side components are the EMI filter, full bridge rectifier, high-frequency inverter, and compensation, also the secondary side is compensation, full bridge uncontrol diode rectifier, and filter. The prototype parameters are taken from Table 3 and the experiment prototype is shown in Figure 19.

Table 3. Structure of coils specification for finite element method (FEM) simulation

Parameter specification	
Primary coil Turns	32
Secondary coil Turns	32
Coil diameter/mm	200 mm
Primary coil Inductance/ μ H	325
Secondary coil Inductance/ μ H	474.22
Ground clearance/mm	120
Mutual inductance/ μ H	62.8
Coil design type	Circular
frequency/kHz	85

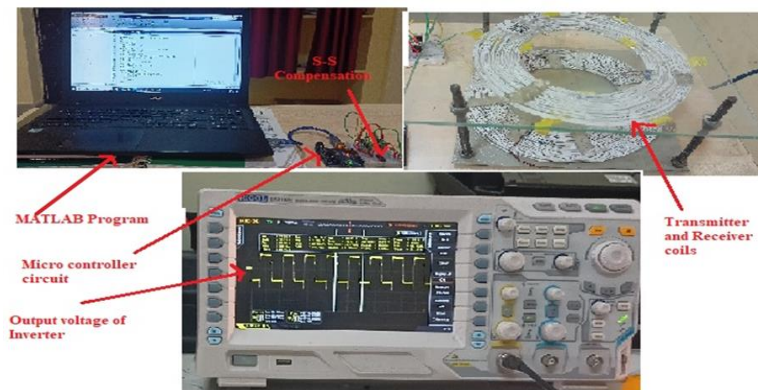


Figure 19 Experiment platform of the S-S compensation modulated WPT system

6. CONCLUSION

A novel receiver-side voltage, current, and power regulated by placing two bidirectional switches are introduced using an S/S compensation topology for the wireless EV charger to reduce the complexity of the power electronic converters. The output power of the secondary side is derived and discussed based on the FHA approach. The deviation of output power with the duty cycle controlled by bidirectional switches is derived and analyzed using MATLAB/Simulink. The simulation results show that output power is controlled, such that with the increase in duty ratio of bidirectional switches the output power is reduced. After validating output characteristics are controlled, in the future for battery charging the constant-current (CC) and constant-voltage (CV) modes will be implemented and more simulation and experimental results will be demonstrated.

ACKNOWLEDGEMENTS

The authors are thankful to the University of Rajiv Gandhi University of Knowledge and Technologies Basar, RGUKT for providing financial and technical support.

REFERENCES

- [1] Y. Mudgal and R. Tiwari, "Impact analysis of integrated renewable energy sources and EVs charging demand on the distribution system," in *2023 IEEE IAS Global Conference on Renewable Energy and Hydrogen Technologies, GlobConHT 2023*, Mar. 2023, pp. 1–5. doi: 10.1109/GlobConHT56829.2023.10087646.
- [2] R. Harikrishnan, P. Sivagami, M. Pushpavalli, G. Rajesh, P. Abirami, and M. Ram, "Evolution of electric vehicle-a review," in *Proceedings - 5th International Conference on Smart Systems and Inventive Technology, ICSSIT 2023*, Jan. 2023, pp. 322–330. doi: 10.1109/ICSSIT55814.2023.10061001.
- [3] P. Vishnuram *et al.*, "Review of wireless charging system: magnetic materials, coil configurations, challenges, and future perspectives," *Energies*, vol. 16, no. 10, p. 4020, May 2023, doi: 10.3390/en16104020.
- [4] V. Saravanan, K. M. Venkatachalam, M. Arumugam, M. A. Borelessa, and K. T. M. U. Hemapala, "Impact of renewable energy in Indian electric power system," *International Journal of Advances in Applied Sciences*, vol. 10, no. 4, pp. 297–309, 2021, doi: 10.11591/ijaas.v10.i4.pp297-309.
- [5] A. Raghuvanshi and A. Ojha, "An overview of the regenerative braking technique and energy storage systems in electric, hybrid, and plug-in hybrid electric vehicles," in *2023 IEEE International Students' Conference on Electrical, Electronics and Computer Science, SCEECS 2023*, Feb. 2023, pp. 1–6. doi: 10.1109/SCEECS57921.2023.10063062.
- [6] H. Polat *et al.*, "A review of DC fast chargers with BESS for electric vehicles: topology, battery, reliability oriented control and cooling perspectives," *Batteries*, vol. 9, no. 2, p. 121, Feb. 2023, doi: 10.3390/batteries9020121.
- [7] Y. Zheng, Z. Y. Dong, Y. Xu, K. Meng, J. H. Zhao, and J. Qiu, "Electric vehicle battery charging/swap stations in distribution systems: Comparison study and optimal planning," *IEEE Transactions on Power Systems*, vol. 29, no. 1, pp. 221–229, Jan. 2014, doi: 10.1109/TPWRS.2013.2278852.
- [8] Z. Zhang and H. Pang, "The era of wireless power transfer," in *Wireless Power Transfer: Principles and Applications*, Wiley, 2022, pp. 1–17. doi: 10.1002/9781119654117.ch1.
- [9] Y. Wang, Z. Sun, Y. Guan, and D. Xu, "Overview of megahertz wireless power transfer," *Proceedings of the IEEE*, vol. 111, no. 5, pp. 528–554, May 2023, doi: 10.1109/JPROC.2023.3265689.
- [10] R. Bhukya and P. S. Kumar, "Performance analysis of modified SVPWM strategies for three phase cascaded multi-level inverter fed induction motor drive," *International Journal of Power Electronics and Drive Systems (IJPEDS)*, vol. 8, no. 2, p. 835, Jun. 2017, doi: 10.11591/ijpeds.v8.i2.pp835-843.
- [11] K. M. Venkatachalam, V. Saravanan, M. A. K. Borelessa, and K. T. M. U. Hemapala, "Single phase seven level Z-source cascaded H-bridge inverter for photovoltaic systems," *International Journal of Advances in Applied Sciences*, vol. 10, no. 1, p. 60, 2021, doi: 10.11591/ijaas.v10.i1.pp60-69.
- [12] D. Li, X. Wu, W. Gao, D. Luo, and J. Gao, "Coupler loss analysis of magnetically coupled resonant wireless power transfer system," *CES Transactions on Electrical Machines and Systems*, vol. 7, no. 1, pp. 63–72, Mar. 2023, doi: 10.30941/CESTEMS.2023.00010.
- [13] J. Rahulkumar *et al.*, "An empirical survey on wireless inductive power pad and resonant magnetic field coupling for in-motion EV charging system," *IEEE Access*, vol. 11, pp. 4660–4693, 2023, doi: 10.1109/ACCESS.2022.3232852.
- [14] W. Li, H. Zhao, J. Deng, S. Li, and C. C. Mi, "Comparison study on SS and double-sided LCC compensation topologies for EV/PHEV wireless chargers," *IEEE Transactions on Vehicular Technology*, vol. 65, no. 6, pp. 4429–4439, Jun. 2016, doi: 10.1109/TVT.2015.2479938.
- [15] H. Ma *et al.*, "Efficiency optimization for LCC-LC compensated inductive coupling power transfer system with load-independent zero-phase-angle and constant voltage output," *International Journal of Circuit Theory and Applications*, Mar. 2023, doi: 10.1002/cta.3591.
- [16] A. Khaligh and S. Dusmez, "Comprehensive topological analysis of conductive and inductive charging solutions for plug-in electric vehicles," *IEEE Transactions on Vehicular Technology*, vol. 61, no. 8, pp. 3475–3489, Oct. 2012, doi: 10.1109/TVT.2012.2213104.
- [17] Z. Zhang, H. Pang, A. Georgiadis, and C. Cecati, "Wireless power transfer - an overview," *IEEE Transactions on Industrial Electronics*, vol. 66, no. 2, pp. 1044–1058, Feb. 2019, doi: 10.1109/TIE.2018.2835378.
- [18] T. D. Nguyen, S. Li, W. Li, and C. C. Mi, "Feasibility study on bipolar pads for efficient wireless power chargers," in *Conference Proceedings - IEEE Applied Power Electronics Conference and Exposition - APEC*, Mar. 2014, pp. 1676–1682. doi: 10.1109/APEC.2014.6803531.
- [19] X. Mou, D. T. Gladwin, R. Zhao, and H. Sun, "Survey on magnetic resonant coupling wireless power transfer technology for electric vehicle charging," *IET Power Electronics*, vol. 12, no. 12, pp. 3005–3020, Oct. 2019, doi: 10.1049/iet-pel.2019.0529.
- [20] C. Cui, X. Gao, S. Cui, and Q. Zhang, "Configuration method and parameter impact analysis of parallel LCC compensation WPT systems," in *Lecture Notes in Electrical Engineering*, 2023, vol. 1018 LNEE, pp. 829–842. doi: 10.1007/978-981-99-0631-4_83.

- [21] X. Xie, C. Xie, J. Wang, Y. Li, Y. Du, and L. Li, "Constant current output control based on cross-coupling compensation in multireceiver WPT system using active rectifier," *IEEE Transactions on Transportation Electrification*, vol. 9, no. 1, pp. 1960–1972, Mar. 2023, doi: 10.1109/TTE.2022.3174016.
- [22] N. Fu, J. Deng, Z. Wang, and D. Chen, "Dual-Phase-Shift Control Strategy With Switch-Controlled Capacitor for Overall Efficiency Optimization in Wireless Power Transfer System," *IEEE Transactions on Vehicular Technology*, vol. 72, no. 6, pp. 7304–7317, Jun. 2023, doi: 10.1109/TVT.2023.3241695.
- [23] D. Wang, C. Fu, X. Bei, and Q. Zhao, "A reconfigurable half-bridge compensation topology-based WPT system with constant current and constant voltage outputs," *IEEE Transactions on Circuits and Systems II: Express Briefs*, vol. 70, no. 1, pp. 256–260, Jan. 2023, doi: 10.1109/TCSII.2022.3206582.
- [24] P. Tan, B. Song, W. Lei, H. Yin, and B. Zhang, "Decoupling control of double-side frequency tuning for LCC/S WPT system," *IEEE Transactions on Industrial Electronics*, vol. 70, no. 11, pp. 11163–11173, Nov. 2023, doi: 10.1109/TIE.2022.3224139.
- [25] Y. Wang, Z. Yang, F. Lin, J. Dong, and P. Bauer, "Frequency tracking method and compensation parameters optimization to improve capacitor deviation tolerance of the wireless power transfer system," *IEEE Transactions on Industrial Electronics*, vol. 70, no. 12, pp. 12244–12253, Dec. 2023, doi: 10.1109/TIE.2022.3232657.
- [26] B. X. Nguyen *et al.*, "An efficiency optimization scheme for bidirectional inductive power transfer systems," *IEEE Transactions on Power Electronics*, vol. 30, no. 11, pp. 6310–6319, Nov. 2015, doi: 10.1109/TPEL.2014.2379676.
- [27] D. Patil, M. K. McDonough, J. M. Miller, B. Fahimi, and P. T. Balsara, "Wireless power transfer for vehicular applications: overview and challenges," *IEEE Transactions on Transportation Electrification*, vol. 4, no. 1, pp. 3–37, Mar. 2017, doi: 10.1109/TTE.2017.2780627.
- [28] S. Li, W. Li, J. Deng, T. D. Nguyen, and C. C. Mi, "A double-sided LCC compensation network and Its tuning method for wireless power transfer," *IEEE Transactions on Vehicular Technology*, vol. 64, no. 6, pp. 2261–2273, Jun. 2015, doi: 10.1109/TVT.2014.2347006.
- [29] G. Feng, Z. Liu, X. Wei, Z. Liu, X. Zhu, and S. Shao, "Study of double-sided LCC compensation wireless power transfer based on zero voltage switching," in *2020 IEEE Student Conference on Electric Machines and Systems, SCEMS 2020*, Dec. 2020, pp. 713–717. doi: 10.1109/SCEMS48876.2020.9352358.
- [30] C. Sen Wang, O. H. Stielau, and G. A. Covic, "Design considerations for a contactless electric vehicle battery charger," *IEEE Transactions on Industrial Electronics*, vol. 52, no. 5, pp. 1308–1314, Oct. 2005, doi: 10.1109/TIE.2005.855672.
- [31] W. Zhang, S. C. Wong, C. K. Tse, and Q. Chen, "Design for efficiency optimization and voltage controllability of series-series compensated inductive power transfer systems," *IEEE Transactions on Power Electronics*, vol. 29, no. 1, pp. 191–200, Jan. 2014, doi: 10.1109/TPEL.2013.2249112.
- [32] Y. Zhang, Z. Yan, T. Kan, Y. Liu, and C. C. Mi, "Modelling and analysis of the distortion of strongly-coupled wireless power transfer systems with SS and LCC–LCC compensations," *IET Power Electronics*, vol. 12, no. 6, pp. 1321–1328, May 2019, doi: 10.1049/iet-pel.2018.5542.
- [33] J. Liu, Y. Zhang, Z. Wang, and M. Cheng, "Design of a high-efficiency wireless charging system for electric vehicle," in *2018 1st Workshop on Wide Bandgap Power Devices and Applications in Asia, WiPDA Asia 2018*, May 2018, pp. 40–44. doi: 10.1109/WiPDAAsia.2018.8734657.
- [34] B. Pang, J. Deng, P. Liu, and Z. Wang, "Secondary-side power control method for double-side LCC compensation topology in wireless EV charger application," in *Proceedings IECON 2017 - 43rd Annual Conference of the IEEE Industrial Electronics Society*, Oct. 2017, vol. 2017-January, pp. 7860–7865. doi: 10.1109/IECON.2017.8217377.
- [35] J. T. Boys, G. A. Covic, and A. W. Green, "Stability and control of inductively coupled power transfer systems," *IEE Proceedings: Electric Power Applications*, vol. 147, no. 1, pp. 37–42, 2000, doi: 10.1049/ip-epa:20000017.
- [36] B. Bhavsingh, B. Mangu, and G. S. Babu, "Design and analysis of a high-efficiency dual side S-S compensation topology of inductive power transfer for EV battery charging system," in *2022 IEEE 2nd International Conference on Sustainable Energy and Future Electric Transportation, SeFeT 2022*, Aug. 2022, pp. 1–6. doi: 10.1109/SeFeT55524.2022.9908627.
- [37] M. K. Thukral, "Design and Simulink implementation of electrical vehicle charging using wireless power transfer technology," in *Lecture Notes in Electrical Engineering*, vol. 648, 2020, pp. 631–640. doi: 10.1007/978-981-15-2926-9_69.
- [38] J. Thalapil Vaheeda and B. George, "In-Vehicle Sensing System to Sense the Ground Pad Configuration in the V2G Mode of EV," *IEEE Sensors Journal*, vol. 23, no. 9, pp. 10080–10088, May 2023, doi: 10.1109/JSEN.2023.3260198.

BIOGRAPHIES OF AUTHORS



Bhukya Bhavsingh     is an Assistant Professor in the Department of Electrical and Electronic Engineering, RGUKT-IIIT, Basara, Telangana, India. He obtained a B.Tech in Electrical and Electronics Engineering from Vaagdevi College of Engineering, Warangal in 2009 and an M.Tech in Power Electronics in 2012 from Vaagdevi College of Engineering Warangal. He Pursuing a Ph.D. in the Department of Electrical Engineering, University College of Engineering, Osmania University, Hyderabad, INDIA. His research interests include power electronics, DC-DC converters, electrical vehicles, and wireless transmission. He has more than 5 Publications in International Journals and has Attended and Presented Papers in National Conferences. He can be contacted at email: bhavsingh.eee@rgukt.ac.in.



Gotluru Suresh Babu     is a professor of Electrical Engineering at the Department of Electrical and Electronics Engineering and Chaitanya Bharathi Institute of Technology (CBIT), Hyderabad. He received a Ph.D. in 2013 and a master's degree in Electrical engineering from Osmania University Hyderabad in 2001. His research interest is electric drives, energy management, and renewable energy. He can be contacted at email: gsureshababu_eee@cbit.ac.in.



Bhukya Mangu     is a professor of Electrical Engineering at the Department of Electrical Engineering and Process, University College of Engineering, Osmania University Hyderabad. He received a Ph.D. in 2016 from IIT Bombay and a master's degree in Electrical engineering from University University College of Engineering (OU) in 2002. His research interest is renewable energy, electric vehicles, and power electronics converters. He can be contacted at email: mangu.b@uceou.edu.



Ravikumar Bhukya     is an Assistant Professor in the Department of Electrical and Electronic Engineering, RGUKT-IIIT, Basara, Telangana, India. He obtained B.Tech in Electrical and Electronics Engineering from JNTUH in 2010 and M.Tech in Power and Industrial Drives in 2013 from JNTUH. He submitted his Ph.D Thesis on 13th July 2023 waiting for Viva-Voce in the Department of Electrical Engineering, University College of Engineering, Osmania University, Hyderabad, INDIA. His research interests include power electronics, drives, power converters, multi-level inverters, EVs, Wireless Transmission, and Special Machines. He has more than 10 Publications in International Journals and has Attended and Presented Papers in 6 National Conferences. He can be contacted at email: ravikumarb.phd@uceou.edu.